S7-1-3

EFFECT OF MICRO- AND NANO-CRACKS FOR THE MECHANICAL PROPERTIES OF CEMENTITIOUS MATERIALS

Huang Hsing PAN
Prof., Dept. of Civil Engineering, Kaohsiung University of Applied Sciences, Taiwan

Yu Wen LIU
Prof., Dept. of Civil and Water Resources Engineering, National Chiayi University, Chiayi, Taiwan

Fong Yu WU
Inspector, Southern Region Inspection Office, Council of Labor Affairs, Taiwan

ABSTRACT:
This paper concerns on the mechanical properties of cementitious materials affected by micro and nano-cracks based on SEM measurements. Two cement binders with and without nano silica powders are tested. Crack length and crack density of materials subjected to 0, 0.3 f_c', 0.5 f_c', 0.8 f_c' and 1.0 f_c' were measured. Results show that energy absorption, compressive stress and fracture toughness of cementitious materials increase first and then decrease when nano powders continue to increase. Compressive strength is not sensitive to micro and nano-crack density but crack length, and fracture toughness always increases with increasing microcracks before the saturated cracks reach.
Keywords: micro-crack, cementitious materials, compressive stress, toughness

1. INTRODUCTION

Many literatures have been pointed out that adding nano powders into the material can enhance the material properties such as high strength, high rigidity and low water absorption for polymers, and the higher hardness, the toughness and the abrasion for ceramics. Some nano-particles provide a chemical reaction with CH to solidify the voids and microcracks inside concrete [1]. Sometimes, those particles can be treated as the admixture to fill with the pores so as to strengthen the material properties of concrete. Among them, most researchers concentrated on the density, durability, strength and fracture toughness of cementitious materials containing nano particles, and seldom considered the micracracks effect induced by nano particles [2].
Here, we add different volume fractions of nano silica powders to two cement binders, and utilize SEM to observe the micro- and nano-cracks. The strength, fracture toughness and energy absorption of nano silica/cement materials corresponding to the crack density and crack length are discussed.

2. EXPERIMENTAL PROGRAMS

2.1 Materials

Cementitious materials consist of cementitious binder, nano powders and microcracks. Two cement pastes are tested and treated as the binder. One is of 100% cement paste, and the other consists of 80wt% cement and 20wt% slag. A water-to-binder ratio is 0.36 for both binders. Four contents of nano silica powders are considered in the binders with volume fraction of 0.2%, 0.4%, 0.6% and 1% respectively. The average diameter of the nano silica powder is 25nm approximately. The mixture proportions of cementitious materials with w/b=0.36 are shown in Table 1. In Table 1, for example, S-0.2 material consists of 100% cement binder and 0.2vol% silica powders, and SF-0.2 is the binder with 80wt% cement and 20wt% slag and also 0.2vol% silica powders.

Table 1 Mixture proportions (kgf/m^3)

No.	Water	Cement	Slag	Silica powder
S-0	531	1475	0	0
S-0.2	530	1473	0	5
S-0.4	528	1468	0	10
S-0.6	527	1465	0	16
S-1.0	525	1459	0	26
SF-0	525	1166	292	0
SF-0.2	524	1164	291	5
SF-0.4	523	1161	291	10
SF-0.6	522	1159	290	16
SF-1.0	520	1154	289	26

2.2 Measurement

Two sizes with 50×50×50mm and 40×40×160mm were taken to make the specimen. Measured properties of cementitious material include its compressive strength, stress-strain curve, fracture toughness, and energy, respectively, at the material age of 28 days.
For the size of 50×50×50mm, we measured the longitudinal and lateral strain, and plotted the stress-strain curve of the specimen under a uniaxial compression by MTS machine at a constant strain rate

1×10^{-5}/sec. The specimen size with 40×40×160mm was under three-point bending test to calculate the fracture toughness. All data are the average value of six specimens at least.

2.3 SEM Observation

Here, we used SEM to measure the length and quantity of the crack inside cementitious materials under the uniaxial compression with no load, $0.3\,f_c'$, $0.5\,f_c'$, $0.8\,f_c'$ and $1.0\,f_c'$ respectively, where f_c' is the peak strength of the material, and also calculated the crack density. The size of SEM specimens was about 3×3×1.5mm. The observation position of SEM was in the central part of the specimen. Each observation point was examined with three magnifications: 1,000×, 8,000× and 50,000×.

2.4 SEM Image

To take account of the crack properties of cementitious materials, we use Photoshop7.0 software to deal with the SEM image into white and black color, and SigmaScan Pro5 software to count on the number and the length of cracks. Besides, the window size of the crack region was also measured. Figure 1 is the SEM image at a magnification of 8,000×, and Fig. 2 is a black-white conversion of Fig.1. In Fig.2, twelve cracks were counted instead of two in the calculation of crack density here.

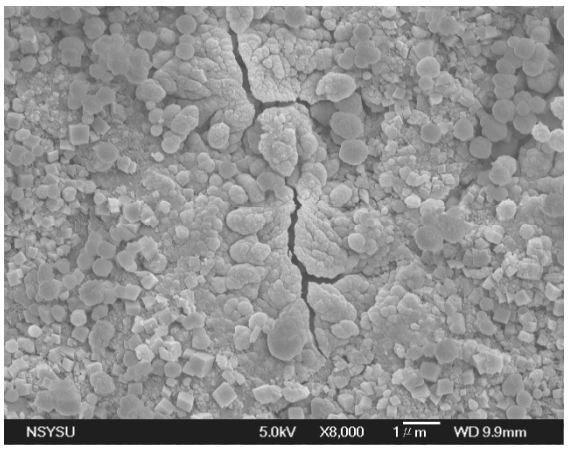

Fig.1 SEM-image of cracks with 8,000×

Fig.2 Black-white conversion of Fig.1

3. THEORETICAL CALCULATION

3.1 Crack Density

Attiogbe and Darwin [3] proposed an analytical procedure used to convert two-dimensional crack data into three-dimensional crack distributions in cement paste and mortar, and concluded that the degree of anisotropy K is about -0.15 when the compressive strain is less 0.002. Thereby, the cracked cement paste and mortar can be taken as an isotropy if the deformation is small.

To calculate the crack density of cementitious materials, let SEM specimens can represent the realistic distribution of cracks inside the material, and all cracks be convex and the same size. Then, a method for the two-dimensional cracks is introduced to determine crack density as [4]

$$\eta = \frac{8}{\pi^3} M \cdot \langle l \rangle^2 \tag{1}$$

where $< l >$ = average trajectory of the cracks and M = total crack number per unit area in SEM window. Let n, h and w be referred as crack number, and the height and the width of SEM window, respectively. Total crack number per unit area then is determined by

$$M = \frac{n}{h \times w} \tag{2}$$

Here, a straight crack means one crack and a bending crack implies the other crack in the calculations. For example, there are 12 cracks shown in Figure 2 in the count.

3.2 Elastic Moduli and Fracture Toughness

Pan and Weng [5] used the inclusion theory [6] to derive the effective elastic bulk modulus κ and effective elastic shear modulus μ of two-phase composite, and found that the elastic moduli of isotropic cracked materials are less sensitive to the crack shape. Here, the binder with nano particles is treated as the matrix (no cracks inside) and the crack as the inclusion. Therefore, we determine the effective elastic moduli of cementitious materials containing circular cracks with the form

$$\frac{\kappa}{\kappa_0} = \frac{3\kappa_0(3\kappa_0 + 8\mu_0) - 2{\mu_0}^2}{3\kappa_0^2(3+8\eta) + 8\kappa_0\mu_0(3+4\eta) - 2{\mu_0}^2} \tag{3}$$

$$\frac{\mu}{\mu_0} = \frac{45(9\kappa_0^2 + 9\kappa_0\mu_0 + 2{\mu_0}^2)}{27\kappa_0^2(15+16\eta) + 3\kappa_0\mu_0(135+256\eta) + 2{\mu_0}^2(45+128\eta)} \tag{4}$$

where κ_0, μ_0 and ν_0 are referred as elastic bulk modulus, elastic shear modulus, and Poisson's ratio of the matrix (no cracks), respectively.

The fracture toughness of the cementitious material can be expressed by the critical stress intensity factor K_c.

Let the stress intensity factor of the matrix, the stress intensity factor near the crack-tip of the cementitious composite and the stress intensity factor change (toughness chance) be denoted as K_0, K_{tip} and ΔK, respectively. The relation of these stress intensity factor is $K_{tip} = K_0 - \Delta K$ and $K_c = K_0 + \Delta K$.

For a two-phase isotropic composite under Mode **I** loading, the analytic solution of toughness change is expressed by [7]

$$\frac{K_{tip}}{K_0} = f\sqrt{g} \tag{5}$$

where f and g are material parameters. It is noted that, in Eq. (5), the ratio K_{tip}/K_0 less than one implies material toughening. If the material contains circular cracks, the material parameters in Eq. (5) are

$$f = \frac{27 + 96k_1(1+\nu_0)^2\eta}{27 + 4(1+\nu_0)^2\eta} \tag{6}$$

$$g = \frac{45(2-\nu_0)[45(2-\nu_0) + 16(1-\nu_0^2)(10-3\nu_0)]}{45(2-\nu_0)^2[45 + 32(5+\nu_0)\eta] + 1024(1-\nu_0^2)(5-\nu_0)(5-2\nu_0)\eta^2} \tag{7}$$

where k_1 = contour factor for main crack. For the steady-state propagating crack, the value of k_1 =0.072. Once we know the crack density of cementitious materials, from Eq. (5), the stress intensity factor increase is determined.

4. RESULTS AND DISCUSSION

4.1 Crack Effect

To investigate the micro- and nano-crack effect, we first need to define the critical length of the crack L_{cri} calculated from the stress intensity factor at the fracture stress σ_c condition, and the form is

$$L_{cri} = \frac{(K_c / Y\sigma_c)^2}{\pi} \tag{8}$$

where Y is the shape parameter of specimen. When the cracks length inside the material is greater than critical length L_{cri} before the loading, this crack dominates the material fracture, not the critical fracture stress, vice verse. This means crack length will affect the strength and toughness of cementitious materials.

The crack density and the length of cementitious materials containing five volume fractions of nano silica powders, 0%, 0.2%, 0.4%, 0.6% and 1%, are measured under the applied stress 0, 0.3 f_c', 0.5 f_c', 0.8 f_c' and 1.0 f_c', respectively. To distinguish the crack length, we divide the measured cracks into two groups: the microcrack (and nano crack) is measured from SEM with the magnification of 8,000× and 50,000×, and the general crack with the magnification of 1,000×, respectively.

Figs. 3-7 show the difference of microcrack density and general crack density of cementitious materials (S), where the parentheses represent average crack length.

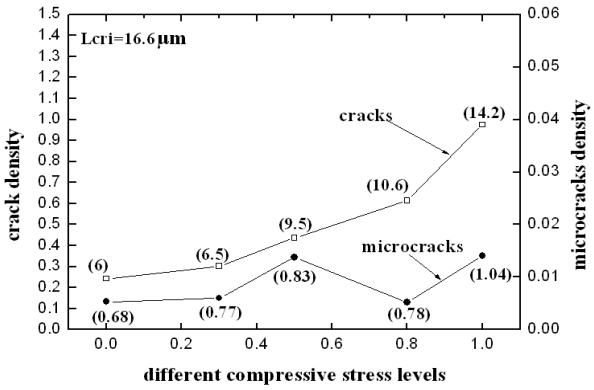

Fig.3 Crack and microcrack density for S-0

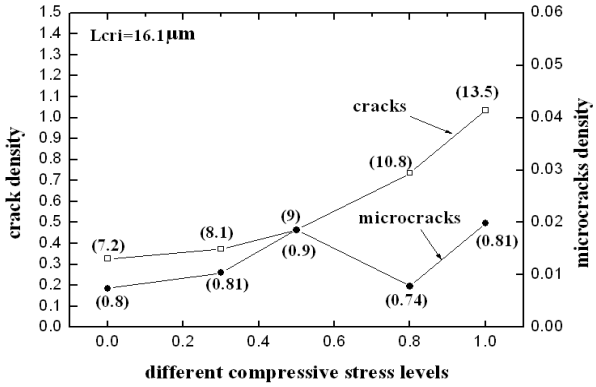

Fig.4 Crack and microcrack density for S-0.2

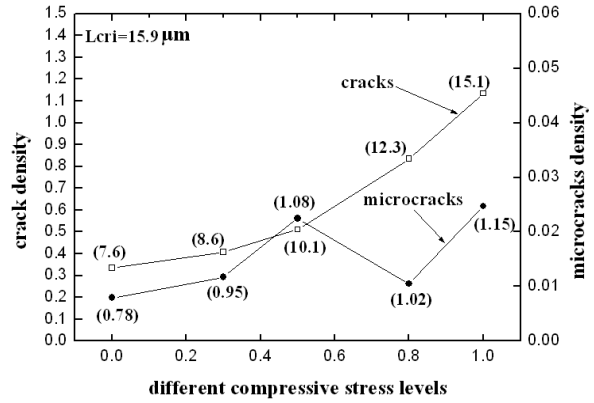

Fig.5 Crack and microcrack density for S-0.4

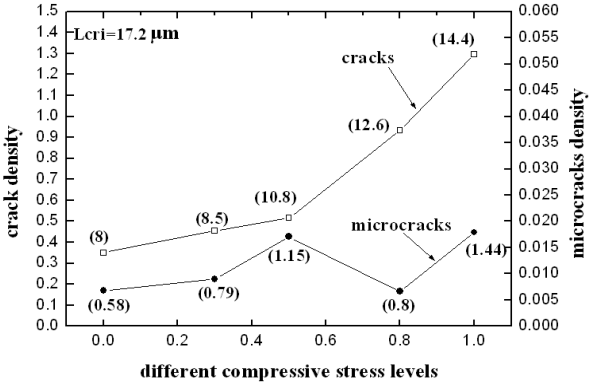

Fig.6 Crack and microcrack density for S-0.6

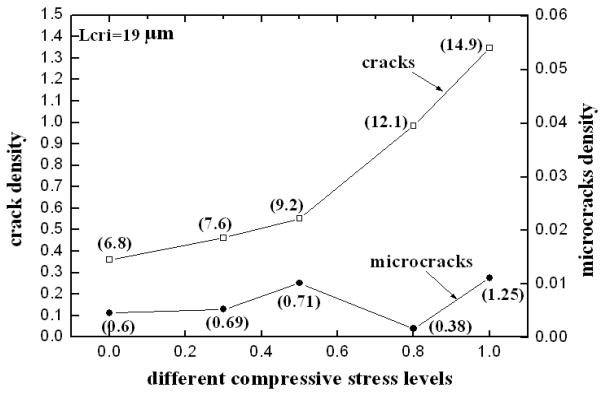

Fig.7 Crack and microcrack density for S-1.0

We compare the influence of general cracks depicted in Figs. 3-7 first. The general crack density continues to increase while the applied stress increase, no matter what volume concentration of silica powders. The increasing tendency of crack density is slow within the applied stress from 0 to 0.5 $f_c^{'}$, and then the curve raises rapid in the range of 0.5 $f_c^{'}$~0.8 $f_c^{'}$. At the higher stress level, 0.5 $f_c^{'}$~0.8 $f_c^{'}$ range, the cracks links together to form a bigger crack, for example S-0.4 material in Fig. 5, the crack length with 7.6μm at applied stress 0 continue to grow to 15.1μm at the peak stress 1.0 $f_c^{'}$.

Meanwhile, the general crack densities in S-0.2, S-0.4, S-0.6 and S-1.0 material shown in Figs. 4-7 are always greater than those in S-0 one in Fig. 3 before the peak stress. From SEM observation, as the volume concentration of nano silica powders increase, nano powders will congregate together induced extra general cracks and microcracks. More micro and nano cracks inside the material are easy to link-up, and become the general cracks at loading. This is the why using nano powders to strengthen cementitious materials have a critical content (threshold) in use. For S-group material, the optimum volume fraction of nano silica powders is S-0.4 material.

All critical crack length L_{cri} calculated from Eq. (8) are greater than average crack lengths at fracture, and the values are shown in Figs 3-7. For instance, the critical length L_{cri} for S-0.4 is 15.9 μm, and the general crack at fracture is 15.1μm, shown in Fig. 5.

For the microcrack case, microcrack densities for S-group materials, shown in Figs. 3-7, increase slowly at 0.3 $f_c^{'}$, then rapid increase at 0.5 $f_c^{'}$, and after that, transform to decrease at 0.8 $f_c^{'}$. In Figs. 3-7, microcrack densities at the stress 0.5 $f_c^{'}$ are all close to and below those at 1.0 $f_c^{'}$. Within 0.5 $f_c^{'}$ ~ 0.8 $f_c^{'}$ range, microcracks are co-linked together to form a bigger crack (general crack) so that the curves of microcrack density drop fast, for example shown in Fig. 5, microcrack density reduces from 0.0225 to 0.0105 for S-0.4 material. When the applied stress increases from 0.8 $f_c^{'}$ to 1.0 $f_c^{'}$, the curves of microcrack density raise again from 0.0105 to 0.0247 shown in Fig. 5.

For the effect of nano silica powders, S-group materials at applied stress 0.5 $f_c^{'}$ shown in Figs. 3-7, the value of microcrack density for S-0, S-0.2, S-0.4, S-0.6 and S-1.0 is 0.0138, 0.0186, 0.0225, 0.0171 and 0.0102, respectively. Microcrack density is the largest at 0.4% volume fraction because the distribution of silica powder is more uniform and less congregate. For the content of 0.6% and 1% silica powders, microcrack density reduces again due to particle congregation.

To distinguish the general crack length and microcrack length in S-group materials, microcrack length is between 0.58 to 1.44μm, and the length of general cracks lies in 6.0 to 15.1μm. Microcrack length is almost one tenth of general crack length.

For SF-group materials, results of crack density and crack length are shown in Figs. 8-12, where the matrix with partial slag powders. The tendency of crack density in SF-group materials is similar to that in S-group ones depicted in Figs. 3-7. The general crack densities shown in Figs. 8-12 continue to grow with increasing applied stress. Unlike the general crack density, microcrack densities first increase up to the stress level at 0.5 $f_c^{'}$, then go down at 0.8 $f_c^{'}$, and after that, increase again at fracture.

While we look into the values of crack density for SF-group and S-group materials, crack densities of SF-group materials are higher than those of S-group ones, same as crack length, too. For example, microcrack density is 0.0266 for SF-0.6 and 0.0179 for S-group at fracture. Also general crack length is 16.7μm and 14.4μm for SF-group and S-group, respectively. Both crack lengths corresponding to the critical length L_{cri} are always the less.

As one know, slag powders have capability of filling with the pores inside cement paste such that this matrix has better density and material properties compared with the matrix without slag powders. For SF-group materials, microcracks ease to form surround silica powders because the matrix is less porous. Due to this reason, the optimum volume fraction of silica powders for SF-group materials is 0.6% instead of 0.4% for S-group materials. Therefore, we conclude that the more solid matrix will generate the more microcracks in the cementitious materials, so as to the general crack density is linked by microcracks at applied stress increase. This effect will induce material toughening.

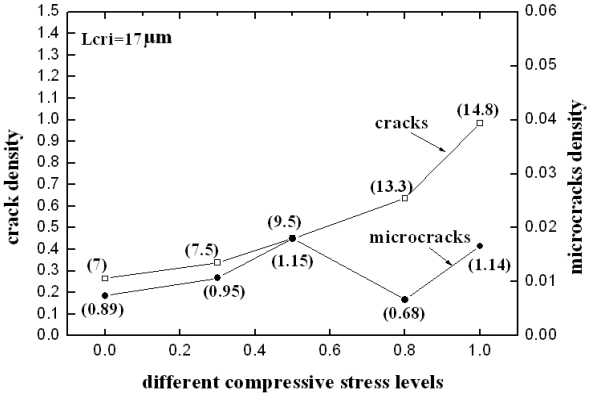

Fig.8 Crack and microcrack density for SF-0

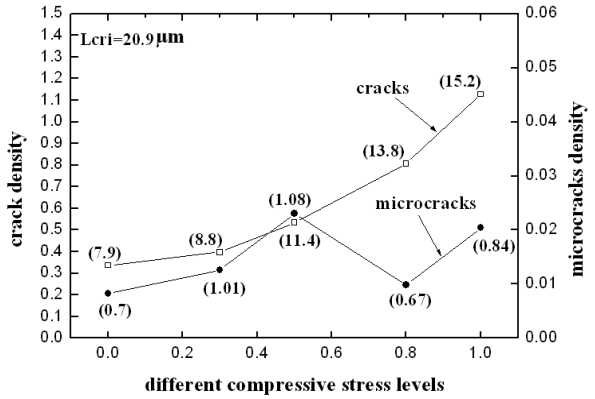

Fig.9 Crack and microcrack density for SF-0.2

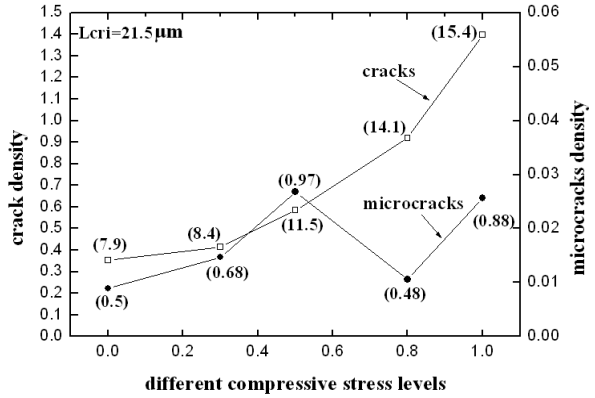

Fig.10 Crack and microcrack density for SF-0.4

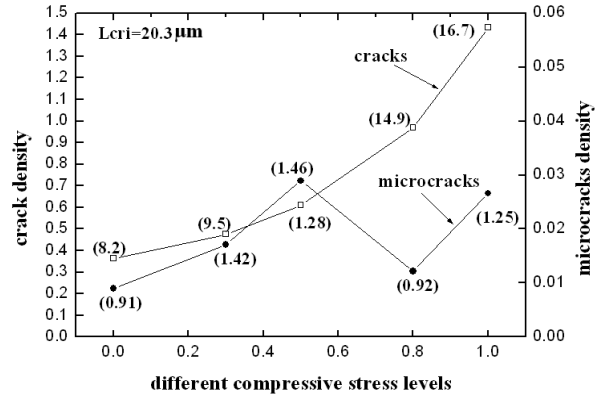

Fig.11 Crack and microcrack density for SF-0.6

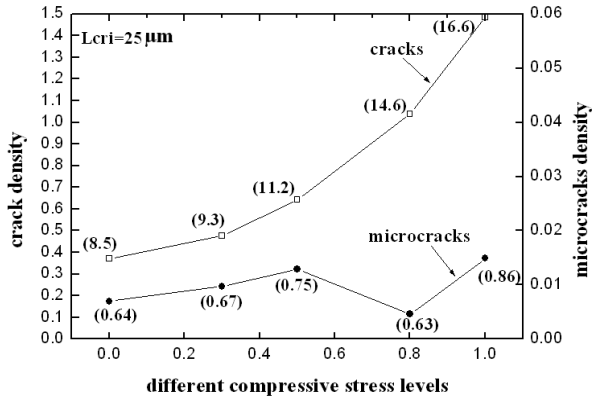

Fig.12 Crack and microcrack density for SF-1.0

4.2 Mechanical Properties

Cementitious materials subjected to the external load generate the general cracks and microcracks inside. We discuss the material properties affected by crack density and crack length.

The force-crack opening displacement (P-CMOD) curves for S-group and SF-group materials are shown in Figs. 13 and 14, respectively. Energy of the materials is calculated from the area under the P-CMOD curve. From Figs. 13 and 14, the S-0.4 and SF-0.6 materials have optimum energy absorption with respect to the maximum microcrack.

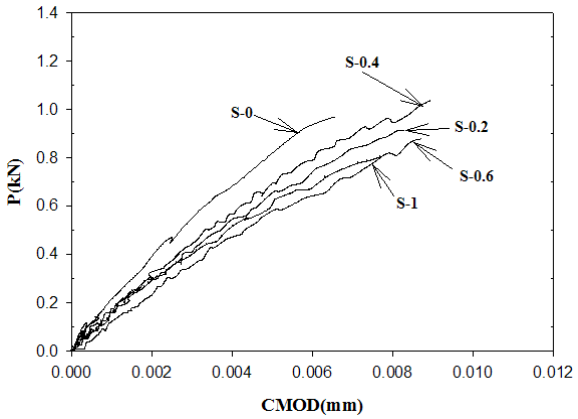

Fig.13 P-CMOD curve for S-group materials

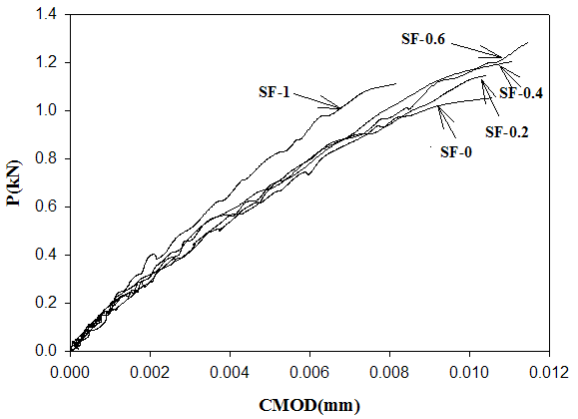

Fig.14 P-CMOD curve for SF-group materials

Table 2 and Table 3 display the mechanical properties related to compressive stress, fracture toughness, energy absorption and the microcrack density at 1.0 $f_c^{'}$. All evidences reveal that the optimum value of the compressive strength, the fracture toughness and energy absorption occurs at the maximum microcrack density or S-0.4 and SF-0.6 materials.

Table 2 Mechanical properties for S materials

No.	Compressive stress (MPa)	Fracture toughness (MPa.m$^{1/2}$)	Energy absorption (N-mm)	Microcrack density
S-0	71.6	0.31	5	0.0140
S-0.2	75.2	0.32	7	0.0198
S-0.4	80.4	0.34	8	0.0247
S-0.6	72.8	0.32	7	0.0179
S-1.0	64.6	0.30	5	0.0112

Table 3 Mechanical properties for SF materials

No.	Compressive stress (MPa)	Fracture toughness (MPa.m$^{1/2}$)	Energy absorption (N-mm)	Microcrack density
SF-0	75.5	0.33	6	0.0166
SF-0.2	76.8	0.39	9	0.0204
SF-0.4	81.2	0.40	9	0.0256
SF-0.6	85.8	0.41	10	0.0266
SF-1.0	66.0	0.35	5	0.0149

The compressive stress of S-1.0 with 64.6MPa is even less that of S-0 without adding nano silica powders. This is because more microcracks link together to become the general crack, and at this moment the crack length is greater than the critical length.

Fig. 15 shows material properties of S-group materials. In this figure, micracracks first increase and then decrease with increasing volume concentration of silica powders, but the measured crack length that greater than the critical crack length becomes longer. S-0.4 material displays the best compressive strength and fracture toughness due to its microcrack density is the maximum. As the volume fractions of silica powders are larger than 0.4%, material properties with respect to compressive strength, energy absorption and fracture toughness are weaken. This means that, if we can create some microcracks but its crack length is less than the critical crack into the brittle materials, we can enhance the toughness of the cementitious materials without affecting the compressive strength.

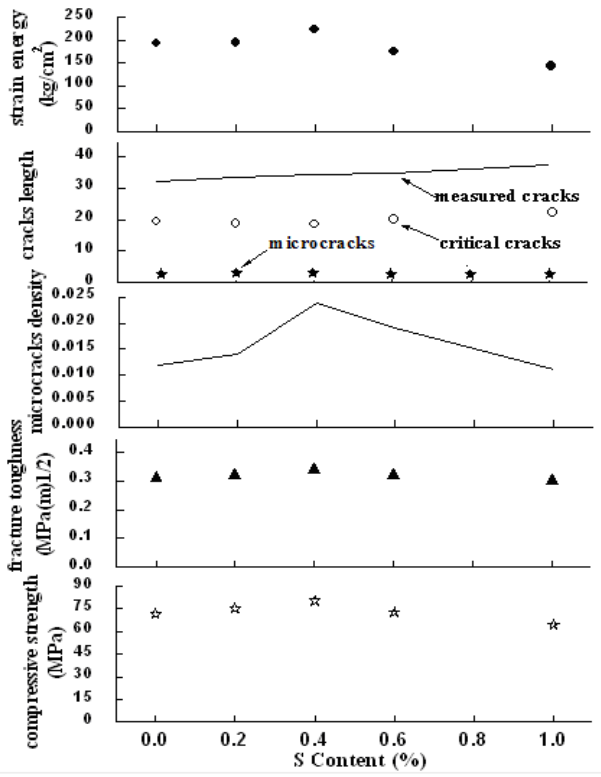

Fig.15 Mechanical properties for S-group materials

Material properties for SF-group materials are shown in Fig.16. Because SF-group materials create more microcracks compared with S-group materials so that material properties of SF-group materials, for example, compressive strength and fracture toughness, are better by comparing Fig. 15 with Fig. 16. The optimum volume fraction of nano silica powders in Fig.16 is SF-0.6, where microcrack density is the maximum.

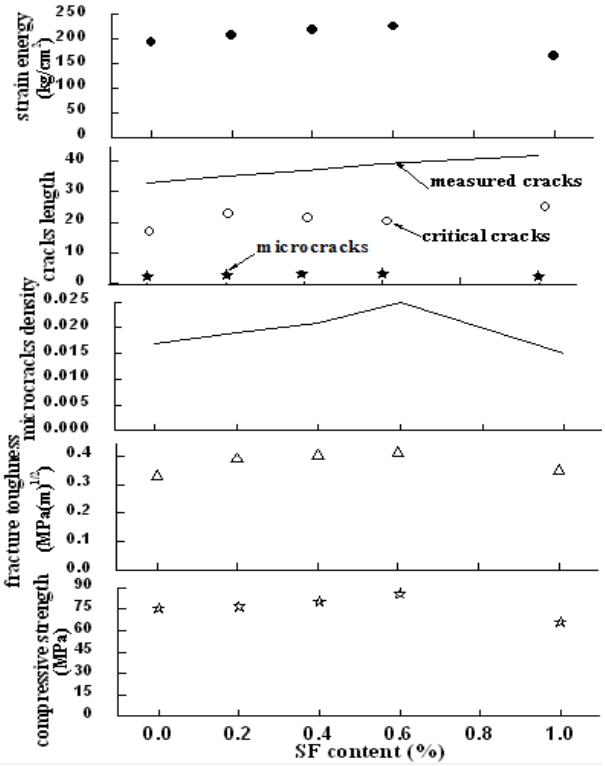

Fig.16 Mechanical properties for SF-group materials

4.3 Theoretical Verification

To verify the experimental data, we calculate the effective elastic bulk moduli and the fracture toughness of cementitious materials from Eq. (3) and Eq. (5). Table 4 shows the results of the calculated results marked by the symbol * and the experimental data. The calculated and experimental data for bulk modulus and fracture toughness are close to each other that confirms the accuracy of the experiments.

Table 4 Mechanical properties of the materials

No.	κ (MPa)	κ^* (MPa)	K_c (MPa m$^{1/2}$)	K_c^* (MPa m$^{1/2}$)
S-0.2	11.8	11.6	0.32	0.31
S-0.4	12.2	12.0	0.34	0.33
S-0.6	11.6	11.5	0.32	0.29
S-1.0	10.6	10.5	0.30	0.29
SF-0.2	11.8	11.6	0.39	0.38
SF-0.4	13.0	12.8	0.40	0.39
SF-0.6	13.5	13.2	0.41	0.37
SF-1.0	10.7	10.6	0.35	0.32

5. CONCLUDING REMARKS

Based on SEM measurements, the compressive strength and the toughness of cementitious materials strong

depend on crack density and crack length. Experimental results show that the best strength and toughness always take place at maximum microcrack density inside the materials. The optimum volume fraction of nano powders is 0.4% in S-group (S-0.4) and 0.6% in SF-group (SF-0.6) materials. The microcrack density of the material applied to the loading continues to increase till 0.5 $f_c^{'}$ and then decreases at 0.8 $f_c^{'}$, but the length and the crack density of the general crack always increase due to the linking of microcracks. Adding applicable microcracks, less than the critical length, into the cementitious material can enhance its toughness without reducing the compressive strength.

ACKNOWLEDGEMENT

The authors would like to thank the Taiwan National Science Council under NSC 97-2221-E-415-011-MY2 for the financial supports.

REFERENCES

1. Andrew, J. A. and Livingstont, R. A., "Relationship Between Differences in Silica Fume Additives and Fine-Scales Microstructural Evolution in Cement Based Materials," Advanced Cement Based Materials, Vol. 8, 1998, pp. 118-131.
2. Takatsune, K. T. and Mihashi, H., "Effect of Artificial Flaws on Toughness of Fiber Reinforced Cementitious Composites", 3rd ACF Int. Conference (ACF/VCA-2008), Nov. 11-13, Ho Chi Minh City, Vietnam, 2008, pp.117-122.
3. Attiogbe, E. K. and Darwin, D., "Correction of Window Size Distortion of Crack Distributions onPlane Sections," J. Microscopy, Vol.114, part1, 1986, pp.71-82.
4. Budiansky, B. and O'Connell, R. J., "Elastic Moduli of a Crack Solid," Int. J. Solids Structures, Vol.12, 1976, pp.81-97.
5. Pan, H. H. and Weng, G. J., "Elastic Moduli of Heterogeneous Solids with Ellipsoidal Inclusions and Elliptic Cracks," Acta Mechanica, Vol.110, 1995, pp.73-94.
6. Weng, G. J., "Some Elastic Properties of Reinforced Solids, with Special Reference to Isotropic Ones Containing Spherical Inclusion," Int. J. Eng. Sci., Vol.22, 1984, pp.845-856.
7. Pan H. H., "An Overall Approach for Microcrack and Inhomogeneity Toughening in Brittle Solids," Chinese J. of Mechanics, Vol.15, 1999, 57-68.